Available online at www.sciencedirect.com
ScienceDirect
Trans. Nonferrous Met. Soc. China 31(2021) 1363−1380
Transactions of Nonferrous Metals Society of China
www.tnmsc.cn

Preparation of bimetallic nano-composite by dissimilar friction stir welding of copper to aluminum alloy

Farhad BAKHTIARI ARGESI, Ali SHAMSIPUR, Seyyed Ehsan MIRSALEHI

Department of Mining and Metallurgical Engineering, Amirkabir University of Technology, Tehran, Iran

Received 18 March 2020; accepted 6 January 2021

Abstract: Butt friction stir welding between pure copper and AA5754 alloy was carried out. Reinforcing SiC nano-particles were utilized in friction stir welded (FSW) joints to decline the harmful effects of intermetallic compounds. Tensile tests, micro-hardness experiments, scanning electron microscopy and X-ray diffraction analysis were applied to studying the properties of welded joints. The joints with a travel speed of 50 mm/min and a rotation speed of 1000 r/min showed the best results. The presence of nano-sized SiC particles reduced the grain size of aluminum and copper in the stir zone (SZ) from 38.3 and 12.4 μm to 12.9 and 5.1 μm, respectively. The tensile strength of the joint in the presence of reinforcing SiC nano-particles was ~240 MPa, which is ~90% of that for the aluminum base. Furthermore, the highest microhardness of the weld zone was significantly increased from HV 160 to HV 320 upon the addition of SiC nano-particles. The results also showed that raising the heat generation in FSW joints increased the amount of Al_4Cu_9 and Al_2Cu intermetallic compounds.

Key words: friction stir welding; dissimilar Al/Cu joint; SiC nano-particles; intermetallic compounds; microstructural characteristics; mechanical properties

1 Introduction

Copper and aluminum are the two available metallic materials that are used in transportation, aerospace, and electrical industries [1]. The interest for industrial applications of aluminum alloys increases due to such important features as an excellent specific, proper corrosion resistance, and low cost. Copper and its alloys are also of critical importance for industrial applications, as they are characterized by suitable thermal expansion, high electrical conductivity, and good corrosion resistance [2]. Nowadays, extensive research has devoted to the joining between dissimilar alloys like copper to aluminum because their joining leads to beneficial properties of both materials [3−6].

AKINLABI et al [2] reported that the dissimilar joining between copper and aluminum is of increasing concern in electrical connections because it reduces the cost and weight of the materials while increasing their life services. Also, researchers [6−8] reported that the dissimilar joining of copper and aluminum using fusion processes is associated with different problems, including the creation of micro-cracking in the welding region as well as such freeze defects as porosity, hot cracking, and a high amount of brittle intermetallic compounds (IMCs), due to the application of high temperatures. Moreover, the fusion welding of aluminum and copper will result in some IMCs, which can weaken the mechanical properties of their joining because of the significant dissimilarity in the chemical and physical properties of the two metals [9,10].

However, to eliminate the drawbacks mentioned above, it has been recommended to perform the welding of copper to aluminum via the

Corresponding author: Ali SHAMSIPUR, Tel: +98-912-5334686, E-mail: Shamsipor@ut.ac.ir
DOI: 10.1016/S1003-6326(21)65583-8

friction stir welding (FSW) as an attractive solid-state welding process [8,11,12]. MISHRA et al [12] reported that the FSW process joins the materials in the solid-state and prevents the occurrence of metallurgical reactions at melting temperature and, therefore, severely reduces the production of IMCs, in comparison with fusion welding. The previous research reports on FSW made it clear that the rotation speed and the welding tool's traverse speed affect the heat generation [13−15]. It has been shown that the heat generation is related to a ratio of the tool rotation (ω) and traverse (v) speeds as ω^2/v [13−15]. Besides the experimental parameters, the welding tool's shape is also a key point to get sound joints. The material flow is affected by the temperature and the tool profile [16,17].

Many researchers [1−3,8,18] confirmed the IMCs formation in FSW between aluminum and copper. Accordingly, the joint's ductility is reduced by the formation of IMCs, due to the inherent nature of the metals, which resulted in reduced yield strength and elongation [18]. MUTHU and JAYABALAN [4] welded the commercially pure copper and AA1100 and reported that a higher strength has resulted from a lower intermetallic phase. MUBIAYI and AKINLABI [3] also reported the formation of some intermetallic compounds, including Al_4Cu_9, Al_2Cu_3, Al_3Cu_4, AlCu, $AlCu_3$, and Al_2Cu in the stir zone of FSWed AA1060 and copper.

One of the attractive techniques that improve the joining properties is the use of reinforcing particles. In this respect, the use of metal matrix composites (MMCs) reinforced with nano/micro-sized particles of low mass, good resistance to corrosion and wear, and excellent mechanical properties at high temperatures are reported in the literatures [19−21]. The addition of reinforcing nano-particles to the joints during the FSW process causes significant changes in the mechanical properties of the joints. In this respect, BAHRAMI et al [22−24] have already conducted several studies on AA7075 joints by adding SiC nano-powders and successfully modifying the SZ with nano-composite structure. Consequently, the mechanical properties such as tensile strength, hardness and tensile fatigue, were improved. Moreover, PANTELIS et al [25], KARTHIKEYAN and MAHADEVAN [26], and ABDOLAHZADEH et al [27,28] reported that the addition of SiC nano-powders strongly affects the FSW process and improves the mechanical properties of the joints.

Meanwhile, BODAGHI and DEHGHANI [29] investigated the effects of SiC nano-particles addition in FSW of AA5052. They reported some improper SiC nano-powder distribution in the premature fracture of the workpieces. SUN and FUJII [30] reported that a uniform distribution of SiC particles in the stir zone of the pure copper joint can be achieved after two passes of FSW. KARAKIZIS et al [31] also studied the effect of TiC and SiC addition on the microstructure, microhardness, and tensile performance properties of AA6082-T6 FSWs. They reported that the SiC particles presented more elongation and made it suitable for applications where a high ductile composite is used. At the same time, the addition of TiC particles resulted in a better microhardness, which made it suitable in applications that need a high wear resistance.

Although several researchers [32−34] have sought to investigate similar FSW of aluminum alloys with reinforcement particles in the stirring zone, a few works have been conducted on the incorporation of nano-particles into a dissimilar FSW process. However, to the best of our knowledge, there has been no previous research report in the literature dealing with the investigation on the effect of producing bimetallic nano-composites in dissimilar friction stir welding of copper to aluminum alloy. Hence, in this study, we investigated the microstructural characteristics and mechanical properties of dissimilar joints between pure copper and AA5754-H114 in the presence of SiC nano-particles.

2 Experimental

In this work, commercially pure copper plates 99.99 wt.% (C10100 OFHC) and 5754-H114 aluminum alloy were used for the friction stir welding with a thickness of 4 mm. The compositions of 5754-H114 aluminum alloy and pure copper are summarized in Table 1. The 45−60 nm SiC particles were used for reinforcing the welded zone in FSW. The properties of SiC nano-particles are shown in Table 2. A threaded tapered H13 heat-treated steel tool used as the FSW tool is shown in Fig. 1.

Table 1 Compositions of AA5754-H114 and C10100 (wt.%)

Material	Si	Fe	Cu	Mn	Mg	Cr	Zn	Al
AA5754-H114	0.16	0.14	0.05	0.33	2.9	0.12	0.09	96.21
Material	Pb	Fe	P	Ag	As	Sb	Zn	Cu
C10100	0.0005	0.001	0.0003	0.0025	0.0005	0.0004	0.0001	99.99

Table 2 Physical and chemical properties of SiC nano-particles

Size range/nm	Purity/wt.%	Bulk density/(g·cm^{-3})	True density/(g·cm^{-3})	Melting point/°C
20−75	>99	0.05	3.2	2730

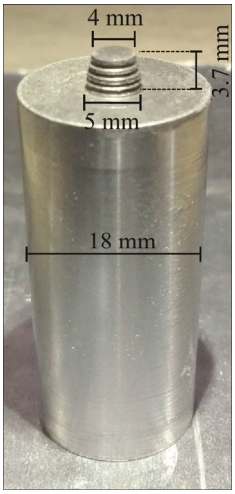

Fig. 1 Welding tool and its dimension

The sheets were cut to dimensions of 20 mm in length and 5 mm in width. The appropriate design was made on aluminum and copper sheets to insert SiC nano-particles into the weld zone. Figure 2 shows a schematic view of the utilized sheets. The SiC nano-particles were added into the groove and pressed tightly; then, the male and female parts of the sheets were brought together. In this way, the nano-particles entirely were placed between the sheets, and no nano-powder dissipation occurred during the FSW process. The possibility of spilling powder out of the groove is eliminated in this connection design. Although the machining and pairing of copper and aluminum sheets were somehow tricky, this was done to eliminate the powder spills.

Also, one pass of the friction stir processing was carried out by a tool without a pin to fix the copper and aluminum sheets and the nano-powder between the sheets before the main welding pass. Consequently, the welding of samples was done in a butt position. Generally, five specimens with the SiC nano-particles and one specimen without the nano-particles were FSWed under the optimal

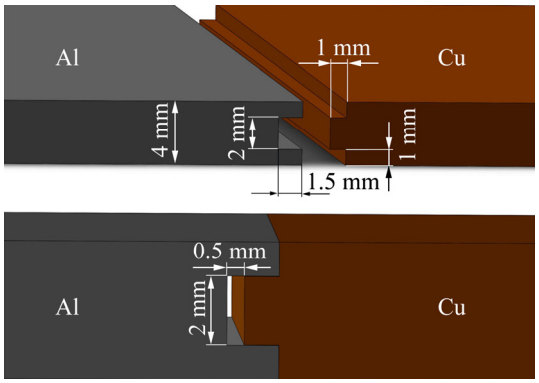

Fig. 2 Schematic of utilized sheets for addition of SiC nano-particles

experimental conditions. In this study, the specimens were labeled. For instance, 800-50 label represents the sample welded with rotating speed of 800 r/min and traveling speed of 50 mm/s. The welding parameters and the welded specimen labels are listed in Table 3. In this work, we used a constant tool, and only the effect of heat generation, due to changes in welding parameters, on the properties of joints was investigated.

Table 3 Welding parameters and FSWed specimens

Sample No.	Specimen code	Use of SiC nano-particles	Rotation speed/(r·min^{-1})	Travel speed/(mm·s^{-1})
1	800-50p	Yes	800	50
2	900-50p	Yes	900	50
3	1000-25p	Yes	1000	25
4	1000-50p	Yes	1000	50
5	1000-100p	Yes	1000	100
6	1000-50	No	1000	50

The aluminum sheet was arranged in the advancing side (AS) and, an offset of 1 mm to the aluminum from the centerline of the joint was used. The plunging time and the tilt angle of the tool were 15 s and 3°, respectively. One of the factors that

affect the weakening of the joint's properties is a weld thinning joint. The high joint efficiency can be attributed to the improvement of the weld thinning joint [35]. The low tool plunge (0.15 mm) was used to reduce the weld thinning.

The microstructure of weldments and weld zone were investigated by optical microscopy (OM). The copper was etched with a mixed solution of 8 mL ammonium hydroxide, 6 mL of hydrogen peroxide, and 12 mL of distilled water. The Barker solution (2.5 vol.% HBF_4) was used to electro-etch the aluminum alloy for 180 s at a voltage of 20 V, and polarized light was used to reveal the grain structure. The X-ray diffraction (XRD) studies were carried out using the Cu K_α X-ray of 1.542 Å wavelength. A scanning electron microscope (SEM) armed with an energy dispersive spectroscope (EDS) was used to analyze the composition of IMCs and distribution of nano-particles in the stir zone. The specimens for the uniaxial tensile test were prepared according to the ASTM E8M-04 standard, and the tensile tests were done at a strain rate of 1 mm/min. The micro-hardness tests of the specimens were performed with a load of 50 g and a dwell time of 10 s according to the ASTM E384-89 on the polished surfaces. The mean grain size of different welded samples' zones was measured matching to the ASTM linear intercept method.

3 Results and discussion

3.1 Macrostructure

Figure 3 shows the appearance of the FSWed 1000-100p specimen. As seen, the tunnel defect is created at the beginning parts of the welding line. ARGESI et al [36] stated that the tunnel creation is attributed to decreasing the heat generation at high tool traveling speeds, which led to insufficient material flow and inadequate mixing of copper in aluminum. Also, DAS et al [37] explained that the welded samples are exposed to severe plastic deformation and thermal cycles by rotating the FSW tool. Thus, such defects as kissing bond and tunnel defect may occur in the welded joint because of insufficient or excessive heat input in the stir zone [38]. Besides, SAREMI et al [39] revealed that increasing traverse speed relative to its normal range created tunnel defects.

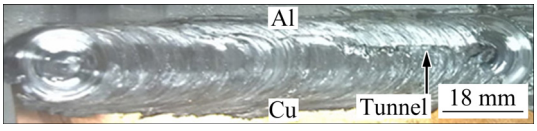

Fig. 3 Appearance of FSWed 1000-100p specimen

The macrostructure of the welded joints' cross-section at different parameters (see Table 3) is shown in Fig. 4. As can be seen, for 1000-100p specimen, a banded layer was observed in the SZ. Due to higher tool traverse speed, material flow and the mixture of aluminum to copper were not adequate, as is visible at lower parts of the FSW joints. Besides, a copper flow is observed near the shoulder. By decreasing the traverse speed, in the 800-50p specimen, the material flow was improved, and consequently, more copper mixing is observed in the SZ. Also, large pieces of copper exist there. As seen, an increase in the tool rotation speed in 900-50p, 1000-50p, and 1000-50 specimens, resulted in an excellent material flow and caused the distribution of more refined copper pieces discontinuously in the cross-sectional macrostructure of the FSW joints. Also, an onion ring pattern is observed for 1000-50p and 1000-50 specimens.

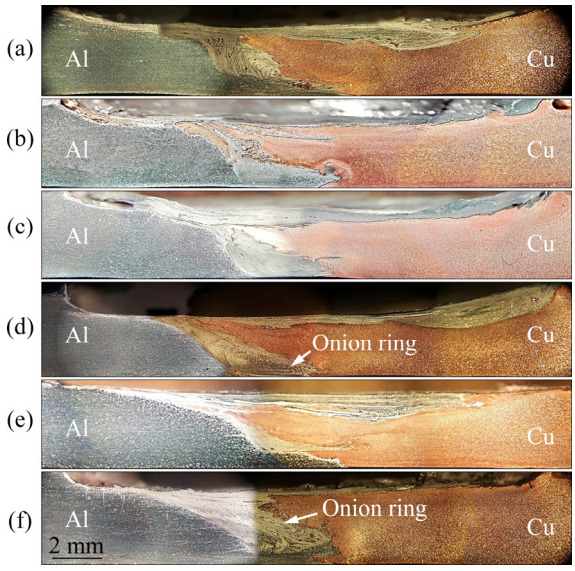

Fig. 4 Macrostructures of FSWed specimens: (a) 1000-100p; (b) 800-50p; (c) 900-50p; (d) 1000-50p; (e) 1000-25p; (f) 1000-50

Furthermore, a finer onion ring formed in the presence of SiC nano-particles in welding of the 1000-50p specimen, compared with the sample FSWed in the absence of SiC nano-particles. It should be noticed that, at the low tool traverse speeds, the heat generation increased and led to a

severe flow of material. This phenomenon resulted in the softening of the SZ and more mixing of copper and aluminum.

The mixing of aluminum and copper for all specimens can be observed. The transfer of materials from copper to aluminum is increased by increasing the extent of heat generation. As can be seen in the SZ of 1000-25p specimen, the amount of copper mixed with aluminum is increased so that the SZ is contained more mixed copper. Tunnel defect was observed in the 1000-100p specimen, indicating the incomplete material mixing between Cu and Al. This was usually associated with insufficient material flow caused by insufficient heat input. With an increase in heat generation, the material flow and mixing between Cu and Al are improved, and defect-free welds containing more mixed copper were obtained. On the other hand, the interaction and consequent inter-diffusion between Cu and Al are increased, which could exacerbate the IMCs and weaken the mechanical properties.

The stir layer pattern is visible throughout the entire section of specimens consisting of aluminum, copper, and IMCs, as examined by SEM. SAHU et al [5] observed an onion-ring pattern in the SZ, which consisted of Al, Cu and their IMCs. The copper pieces separated from the copper bulk were generally spread in the SZ due to inflicted rotation speed. ARGESI et al [36] showed that the SZ of the FSWed joint is an aluminum matrix composite reinforced by copper pieces. The SZ mostly contains aluminum because of the 1 mm tool off-setting into the aluminum side from the centerline of the joint [11]. The pin results in the material movement from the advancing side to the retreating side, while the shoulder area transfers the material from the retreating side to the advancing side.

Consequently, the copper pieces were visible in the upper part of the macrostructure of the specimens. While only the aluminum pieces could be observed at the bottom of the cross-sectional macrostructure of specimens. Also, in the presence of SiC nano-particles, the surface layer of specimens, which is placed precisely under the shoulder, is composed of aluminum and copper due to the groove's design.

3.2 Microstructure

The microstructures of commercially pure copper and AA5754-H114 alloy are shown in Fig. 5. The microstructure of aluminum consisting of non-equiaxed grains, and the copper microstructure shows several annealed twins, as can be noticed within the copper grains. The grain sizes of aluminum and copper were 52 and 36 μm, respectively.

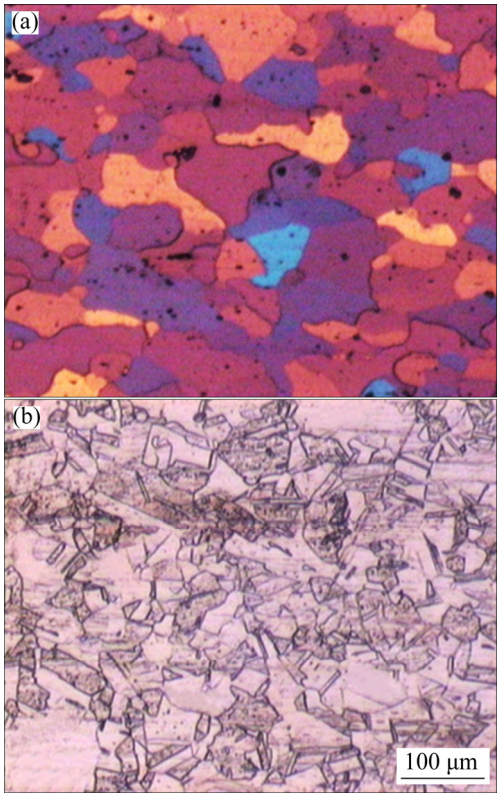

Fig. 5 Microstructures of AA5754-H114 (a) and commercially pure copper (b)

Overall, BAHRAMI et al [24] stated that the microstructure of FSW could be categorized into three regions, including SZ, thermo-mechanical affected zone (TMAZ) and heat-affected zone (HAZ). These three regions for 1000-50p specimen are shown in Fig. 6. In the SZ, more refined grains are observed because of severe plastic deformation. The tool rotation caused the presence of elongated grains in the TMAZ. In the HAZ, the grains grow in FSW due to the heat generation and no plastic deformation.

In the dissimilar friction stir welding of copper and aluminum with the addition of nano-particles, some factors such as dynamic recrystallization, reinforcing of nano-particles, and heat generation control the grain size in the SZ. In all cases, these factors compete with each other to change the grain size. Dynamic recrystallization is the first factor. The low angle grain boundaries change to high

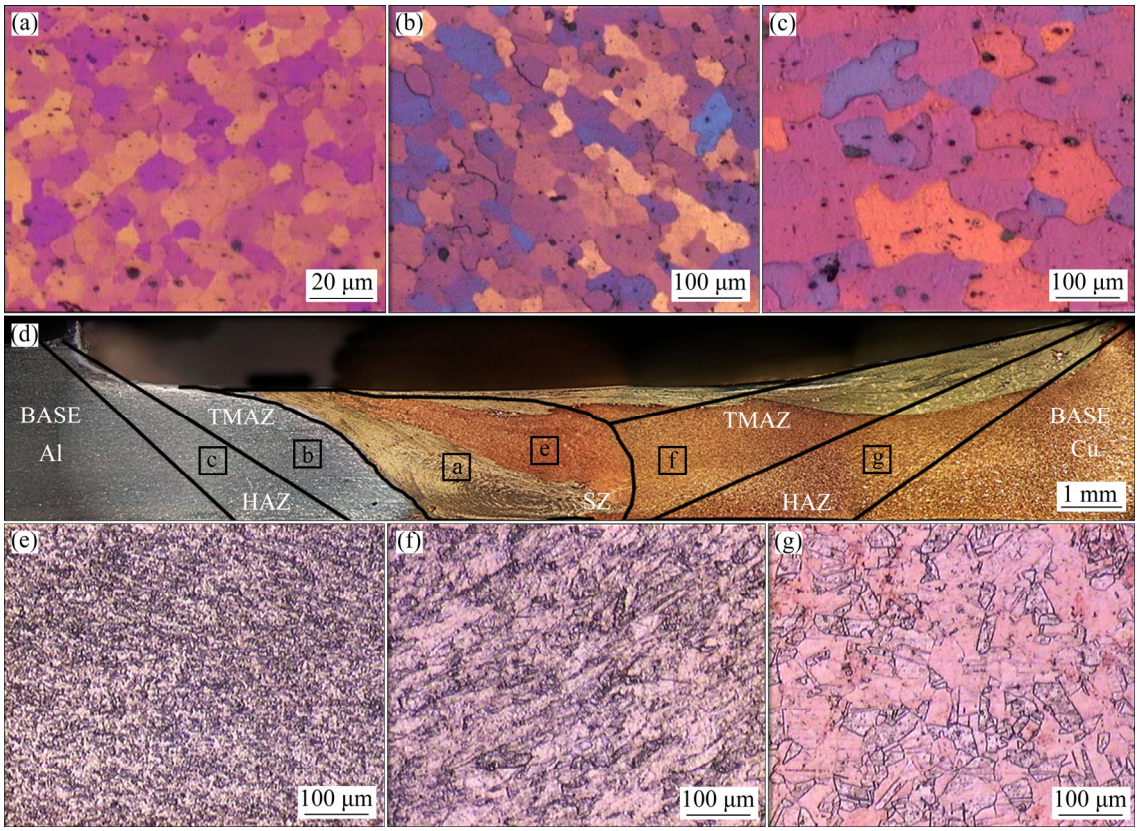

Fig. 6 Various regions for 1000-50p sample: (a) SZ, Al; (b) TMAZ, Al; (c) HAZ, Al; (d) Macrostructure of joint; (e) SZ, Cu; (f) TMAZ, Cu; (g) HAZ, Cu

angle grain boundaries due to the severe plastic deformation and heat generation produced by tool rotation speed during FSW. Thus, the nucleation of new grains occurs in preferred places, which resulted in a reduction in grain size. The effect of reinforcement of nano-particles is a second factor. Reinforced nano-particles could limit the movement of grain boundaries and prevent the grain growth. This is called the pinning effect.

Furthermore, the reinforcement nano-particles can break up the initial grains. As a result, these factors may lead to fine grain structure [22,24,27]. The third factor is the heat generation. ARGESI et al [36] stated that, in the FSW, the friction between the sample and the rotating tool generated the highest amount of heat, which leads to the annealing of the metals, and, as a result, the grain size in the SZ begins to grow.

Figure 7 shows the microstructure of FSWed specimens. All grain sizes evaluated from microstructures are reported in Fig. 8. Two specimens of 1000-50p and 1000-50 were compared together to study the efficiency of SiC nano-particles reinforcements on the microstructure and the grain size of the SZ. As is evident, the addition of SiC nano-particles causes the grain size decreasing of aluminum and copper from 38.3 and 12.4 μm to 12.9 and 5.1 μm, respectively. In fact, in 1000-50p and 1000-50 specimens, the heat generation is constant, and continuous dynamic recrystallization occurs in both specimens. However, reinforcing nano-particles in 1000-50p specimen causes a dramatic decrease in the grain size due to the Zener pinning effect. The reinforcement nano-particles affected the driving force of grain boundary movement by applying the pinning pressure according to the Zener pinning effect.

BODAGHI and DEHGHANI [29] showed that the average grain size of the SZ material would not exceed the critical maximum grain radius (R_c) and the growth of the grains would be restricted. The critical maximum grain radius is given by the equation of $R_c=4r/(3f)$, where r is the radius of reinforcement particles, and f is their volume fraction. Therefore, the fine grains in the SZ were obtained due to the presence of nano-particles incorporated in the joint. ABDOLAHZADEH et al [27] reported that the size of grains reduces

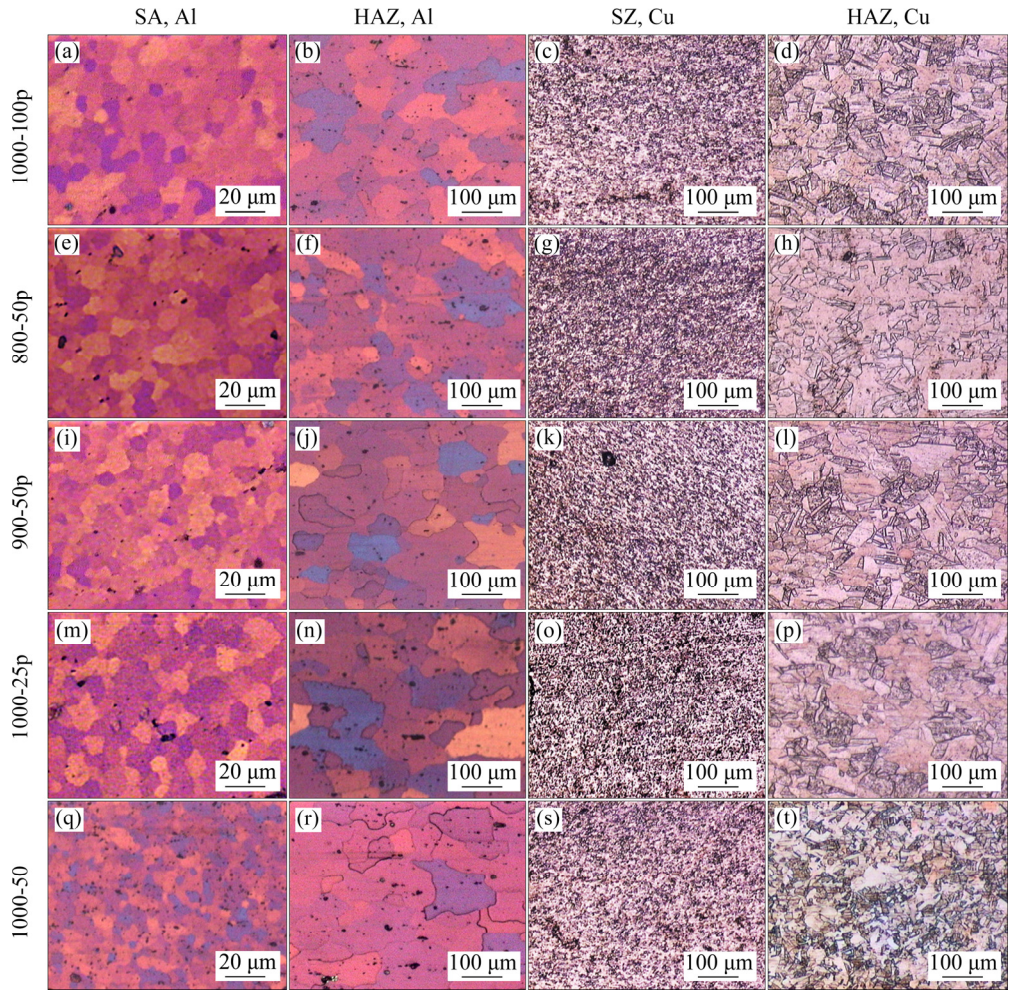

Fig. 7 Microstructures of FSWed specimens

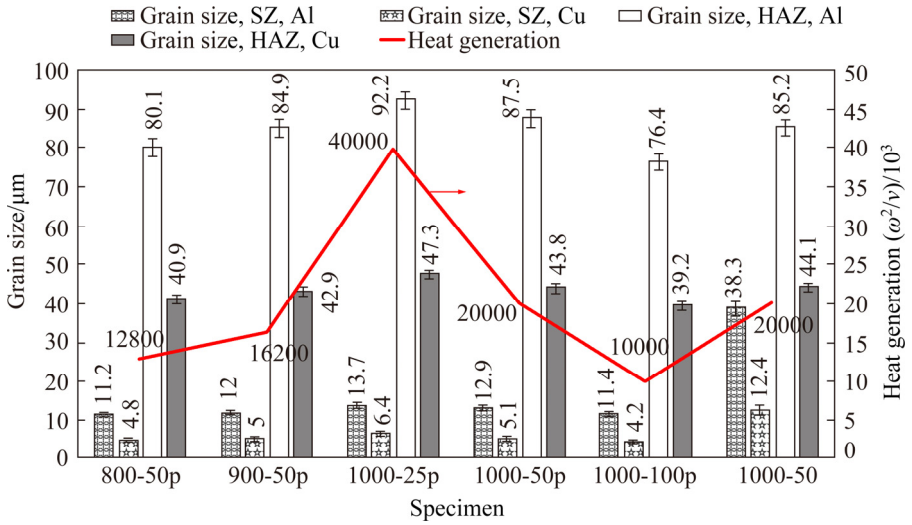

Fig. 8 Grain size of FSWed specimens

from 44 μm in the base to 4 μm in the SZ due to the addition of SiC nano-particles during the FSW. The presence of the SiC nano-particle reinforcements in the SZ exhibited a direct effect on reducing the average grain size. These particles act as ideal nucleation places and also stop the motion of the grain boundaries so that the refining of grains is accrued.

On the other hand, it is observed that a little increase in the grain size occurred by an increase in heat generation. In another word, an increase in heat generation results in grain growth. Two factors of dynamic recrystallization and the addition of SiC nano-particles lead to decreased grain size in specimens. However, increasing heat generation increased the grain size, mainly due to the annealing phenomena. BODAGHI and DEHGHANI [29] have also reported that the increasing heat input causes such an increase in the grain size of the AA5052 sample reinforced by SiC nano-particles.

Also, the grain size in HAZ is only related to the heat generation during FSW. As shown in Fig. 8, the grain sizes in HAZ for 1000-50p and 1000-50 specimens are not different, which is due to the constant heat generation. On the other hand, the grain size of the SZ is increased by enhancing heat input, as is related to grain growth due to annealing, which was reported by ARGESI et al [36] in friction stir welding of pure Cu and AA5754 Al alloy plates. It is visible from Fig. 8, the increase in grain size of copper is much less than that of aluminum. This could be related to the arrangement of the aluminum plate on the advancing side. VERMA and MISRA [40] reported that the temperature in AS is higher than that in the retreating side (RS) due to severer plastic deformation that happened in AS. Also, the coefficient of friction (COF) of aluminum is more than that of copper, and the thermal conductivity of aluminum is lower than that of copper. This causes the rapid cooling of copper and avoids the growing of grains in HAZ.

Figure 9(a) shows an OM image of the onion ring structure within the SZ of 1000-50p specimen, indicating both the particles-free and the particles-rich areas. The formation of intermittent particle-rich and particle-free areas has been previously referred to in several studies [22,27,30]. ABDOLAHZADEH et al [27] remarked that the onion shape structure formed in the stir zone contains SiC-free and SiC-rich regions in the cross-section of FSW joints. It is visible that the SiC-rich regions are darker than SiC-free regions. Figures 9(b) and (c) illustrate the SiC-rich and the SiC-free regions, respectively. As is evident, good distribution and no agglomeration of SiC nano-particles are visible in the SZ 1000-50p specimen.

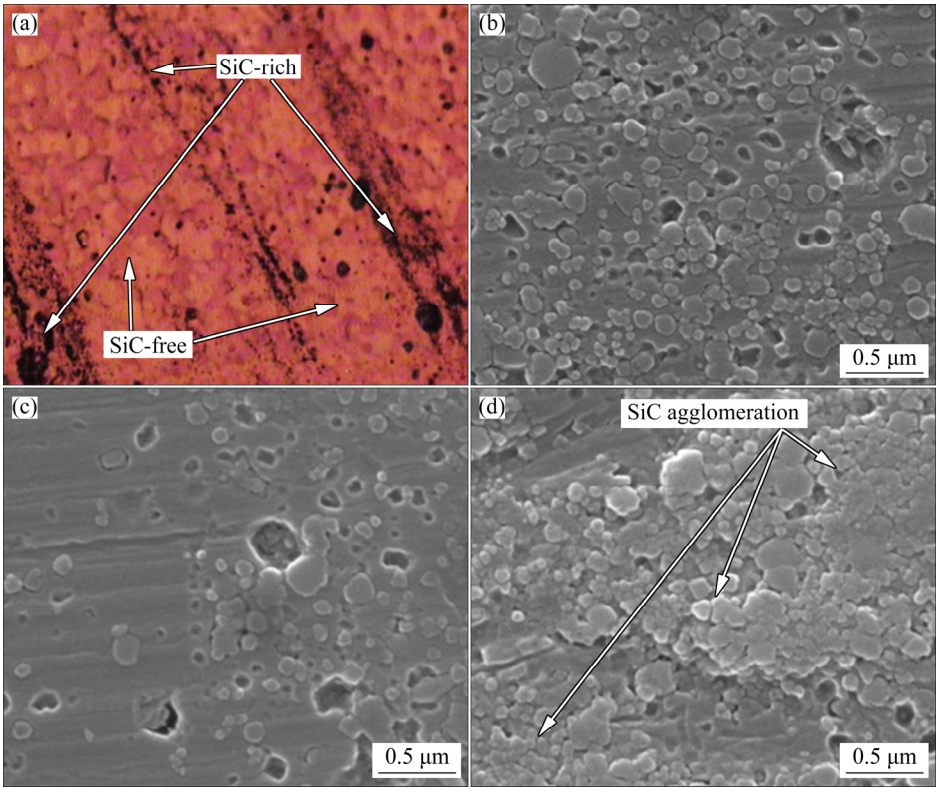

Fig. 9 OM image of SiC-rich and SiC-free regions in 1000-50p specimen (a), SEM image of SiC-rich region in 1000-50p specimen (b), SEM image of SiC-free region in 1000-50p specimen (c) and agglomeration of SiC nanoparticles in 1000-100p specimen (d)

On the other hand, in the 1000-100p specimen, the traverse speed is high, and there is no ample opportunity for incorporation of SiC nano-particles in this joint so that the SiC nano-particles are willing to agglomerate. Figure 9(d) shows such an agglomeration of SiC nano-particles in the FSWed 1000-100p specimen. Generally, the dispersion of nano-sized SiC particles becomes more uniform in the joints by reducing the traverse speed of the tool.

Thus, depending on the rotation speed of welding tool, the incorporation of SiC nano-particles in some regions is more than that in some other regions; hence, the rich and free regions of the SiC nano-particles are created. Moreover, the grain size in SiC-rich regions is finer than that in the SiC-free regions [24,27].

Figure 10 shows the EDS maps of the SZ 1000-50p specimen, which confirm the existence and distribution of SiC nano-particles in the SZ. The uniform distribution of particles in the weldments increases the pinning effects and, consequently, the weld strength. It also clearly shows the uniform particle distribution in 1000-50p specimen. As it is obvious from the results of the microstructure, the grain sizes of aluminum and copper in the 1000-50p specimen decreased from 38.3 and 12.4 μm to 12.9 and 5.1 μm, respectively. The grain refinement of the stir zone is mainly due to the uniform distribution of SiC nano-particles and good stirring effect of the FSP parameters.

3.3 Intermetallic compounds formation

One of the most significant factors, which severely affect the mechanical properties of joints in dissimilar FSW of aluminum alloy and pure copper, is the formation of hard and brittle IMCs. Hereupon, to precisely examine the microstructure characteristics of dissimilar joints between AA5754 and pure copper, the formation of IMCs should be evaluated.

It could be mentioned that, due to the tool rotation, the mixing takes place between aluminum and copper matrix so that some of the Cu pieces detach from the copper bulk and distribute and mix with aluminum matrix, which leads to the formation of IMCs through the solid-state diffusion in the SZ [36]. The chemical reaction between aluminum and copper below the melting point leads to the IMCs formation. The formation of such IMCs depends on the temperature, time, and chemical compositions [6,8,9]. The amount and the type of IMCs depend on the heat generation, the offset value, and the sheets' position, etc. Some analysis was performed on the 1000-100p specimen, in which the heat generation is low, and 1000-50 specimen to investigate the IMCs formation.

Figure 11(a) shows the SEM image of the SZ of 1000-100p specimen. The IMCs are formed at the interface of aluminum and copper, which is black in this figure. EDS analysis was performed at *p*1, and the result is shown in Fig. 11(d).

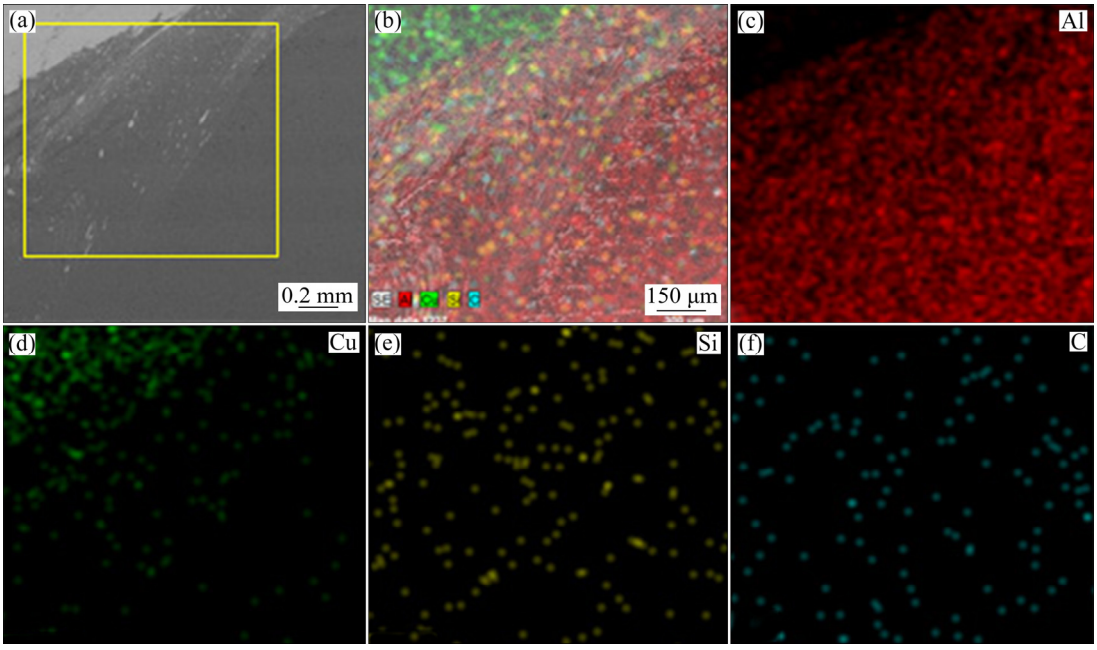

Fig. 10 SEM micrograph of 1000-50p specimen (a) and ESD maps of selected area (b−f)

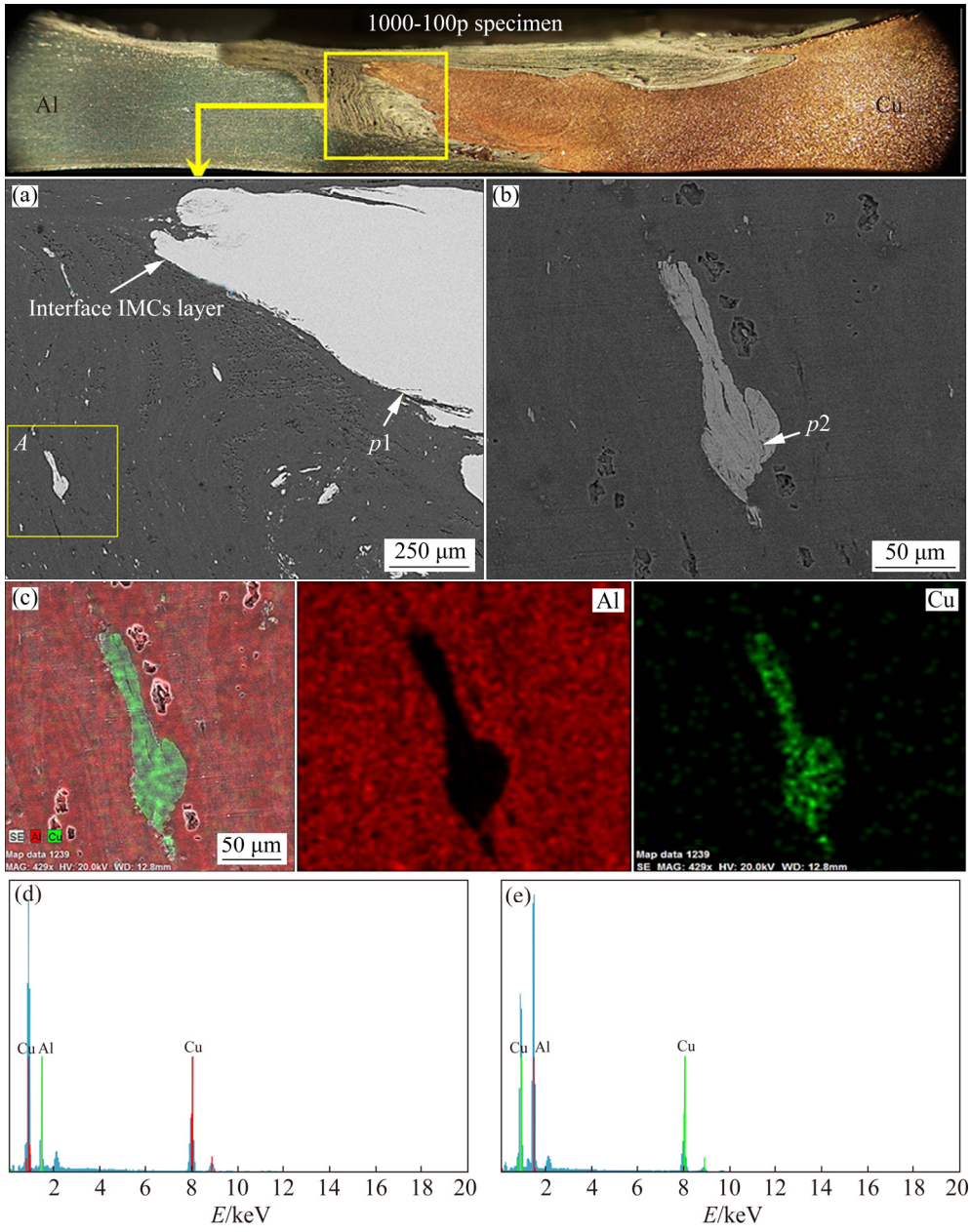

Fig. 11 SEM image of 1000-100p specimen in SZ (a) and higher magnification of Area *A* (b), EDX map at Area *A* and distribution of Al and Cu (c), EDS analysis of *p*1 (d) and *p*2 (e)

Figure 11(a) also shows that the copper segments detached from the Cu plate are distributed in aluminum SZ. Therefore, the weld nugget can be described as an aluminum matrix composite reinforced by pieces of copper. SAHU et al [5] reported that the SZ might be visualized as a composite matrix of aluminum; this is because the stirred copper particles broken and dispersed into the aluminum matrix. Figure 11(b) shows the magnified SEM of region *A* of the large copper fragment, and Fig. 11(c) demonstrates the EDX map of this region. The EDX map revealed the distribution of Cu and Al elements. Therefore, the formation of a tiny IMC layer is also plausible. The EDS analysis was performed on *p*2 to make sure of tiny IMCs formation and percentage of elements, and the result is shown in Fig. 11(e).

Figures 12(a) and (b) show the SEM images of the SZ joint in the two secondary electron and the backscatter electron modes, respectively. The stirred layers are recognizable from Fig. 12(a), consisting of aluminum, copper and IMCs. Figure 12(b) shows the SEM image of copper pieces detached from a copper plate in response to

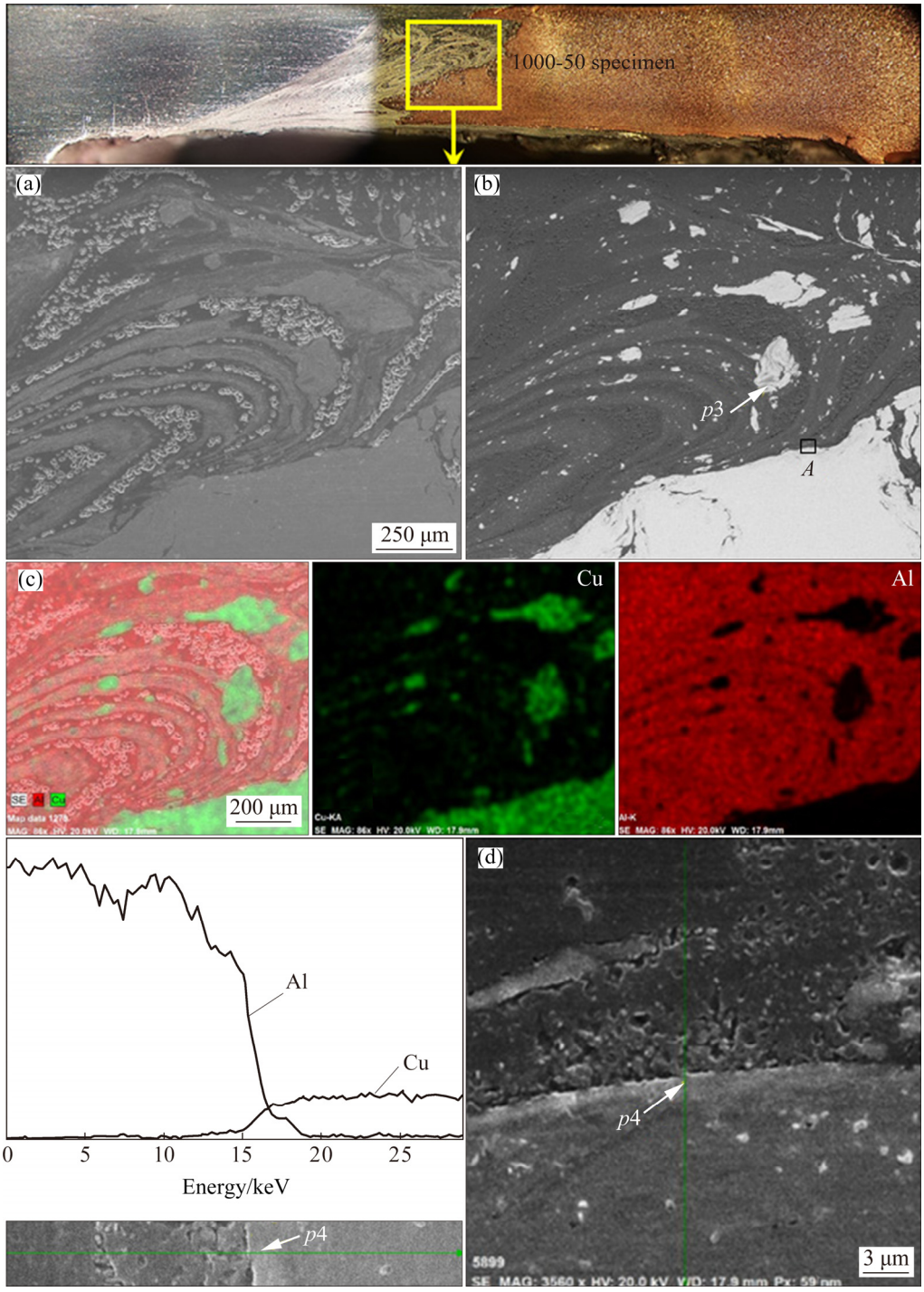

Fig. 12 SEM images of 1000-50 FSWed sample: (a) SZ image in secondary electron mode; (b) SZ image in backscatter mode; (c) EDX map; (d) Linear analysis in Area *A*

the rotational tool, as they are distributed in aluminum SZ. Figure 12(c) shows the EDX map taken from the SZ. The EDX mapping clearly shows the distribution of the aluminum and copper elements. According to the EDX map, the EDS analysis was performed in *p*3 due to the co-presence of aluminum and copper. The linear analysis has already been applied to IMCs formation. It has been shown that, at the interface of aluminum and copper, the amount of aluminum and copper elements is changed due to the influence of solid-state diffusion. Thus, the EDS analysis was applied at *p*4, and the results are shown in Fig. 12(d).

Table 4 summarizes the EDS analysis results. According to the mole fractions of aluminum and copper given in Table 4 and regarding the binary diagram of copper and aluminum, the formation of Al_2Cu and Al_4Cu_9 IMCs can be confirmed, as it has been already reported in our previous study [36].

Table 4 Results of EDS analysis (at.%)

Point	Al	Cu
*p*1	70.3	29.7
*p*2	33.3	66.7
*p*3	32.2	67.8
*p*4	69.5	27.3

MUTHU and JAYABALAN [8] investigated the influence of heat input on the mechanical properties of welded commercially pure copper and AA1100-H14 alloy. They found that the diffusion at the Al−Cu interface is reduced due to the low enough optimized heat input obtained in their work. LEE et al [41] reported the influence of the IMCs on mechanical properties of the FSWed Al−Cu joints. They found that the thickness of the IMCs layer increases with increasing the annealing time. Interestingly, the thickest IMCs were found to increase with increasing dwell time and temperature. The formation and distribution of brittle structures in FSW of aluminum and copper were also studied by GALVAO et al [42]. They found that the solid-state diffusion is strongly influenced by the type and amount of intermetallic phases.

In fact, by raising the heat generation, the SZ will be under severe plastic deformation so that the solid-state diffusion at the copper−aluminum interface is increased, which in turn results in an increase in the amount of the IMCs. Thus, the results obtained in this work well clarified that the IMCs formation increases with increasing heat generation.

From the results of the microstructure analyses, the formation of such IMCs as Al_2Cu and Al_4Cu_9 occurs due to the heat generation of the FSP tool and the plastic deformation in the stir zone.

3.4 Mechanical properties

It is well-known that the mechanical properties of copper−aluminum dissimilar joints could be dependent on different microstructural factors, including dislocation density [22,27], grain size [24,27], and IMCs [8,15,18,41]. However, in the presence of SiC nano-particles, the mechanical properties could be determined by the distribution of hard SiC nano-particles [24,27,29,30]. The mechanical properties of FSW joints obtained in this work, including yield strength (YS), ultimate tensile strength (UTS), elongation, and failure energy, are shown in Fig. 13.

3.4.1 Tensile properties

Since no nano-particles are used in the FSWed joints between aluminum and copper, the tensile properties are mainly related to grain size and the presence of IMCs, as was previously studied by our group [36]. However, the tensile properties are expected to be more different by adding SiC nano-

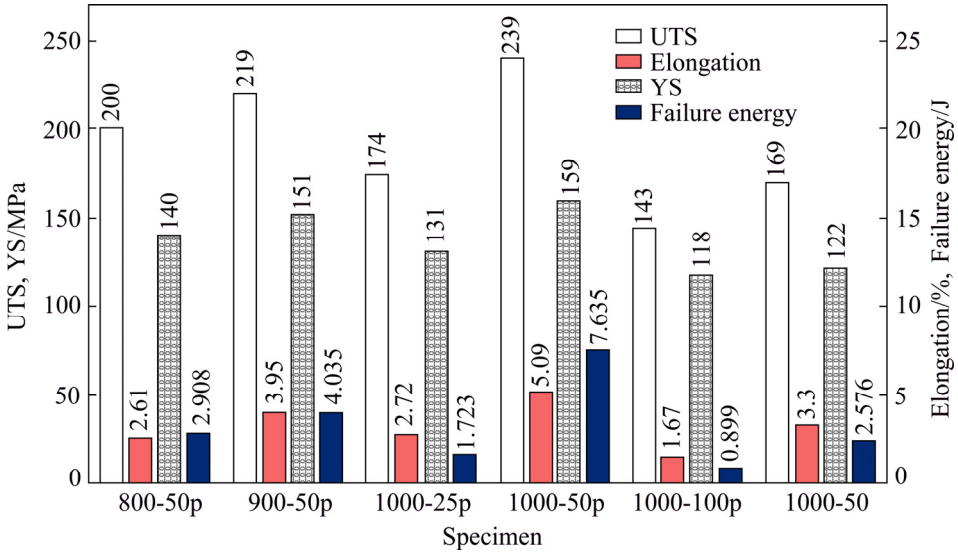

Fig. 13 Mechanical properties of FSWed specimens

particles to joints. The interaction between base metal and reinforcement, degree of particle agglomeration, distribution of particles in the matrix, and the interfacial bond between base metals and reinforcement particles affect the tensile properties [22,24,27,29]. The distribution of nano-particles in the SZ enhances the pinning effects and, consequently, increases the weld strength.

By comparing the 1000-50p and 1000-50 specimens, one can find the effect of adding SiC nano-particles. The tensile strengths of 1000-50p and 1000-50 specimens are 239 and 169 MPa, respectively. In our former work, we found that the low UTS of 1000-50 specimen is related to much IMCs formation due to the high heat generation [36]. When the SiC nano-particles are used in the FSWed joints, the distribution of SiC nano-particles leads to the improved tensile properties. The addition of SiC nano-particle reinforcement causes a nano-composite in the SZ of the welded specimens. The amount of SiC reinforcement of nano-particles in the SZ nano-composite was calculated as about 8%. This nano-composite improved the tensile properties of the sample due to the ability to transfer the applied tension from the weak matrix into the strong nano-size SiC reinforcement. On the other hand, the presence of SiC nano-particles reduced the grain size in the SZ through the grain boundary's pinning effects. The outcome was an increase in tensile strength through the Hall−Patch relationship.

The Hall−Petch and Orowan−Ashby equations clarify these results. According to DIETER and BACON [43], the Hall−Petch equation explained the relation between the strength and the grain size:

$$\sigma=\sigma_i kD^{-1/2} \quad (1)$$

where D is the grain size, σ_i is friction stress, and k is a material constant parameter. Moreover, the effect of inter-particle spacing on the second phase strengthening can be described by the Orowan−Ashby equation:

$$\Delta\sigma\approx k'\lambda^{-1/2} \quad (2)$$

where λ and k' are the inter-particle and a spacing constant, respectively. Considering Eqs. (1) and (2), the strengthening increases by reducing the interparticle spacing and the grain size. Also, decreasing both the interparticle spacing and the grain size increases the ductility and the elongation.

Figure 14 shows the relationship between UTS and the heat generation for specimens with SiC nano-particles. As seen, by rising the heat generation, UTS first increased and then began to decline. Accordingly, there is an optimal amount of heat generation to affect the joints' properties. This is because heat generation affects the formation of IMCs.

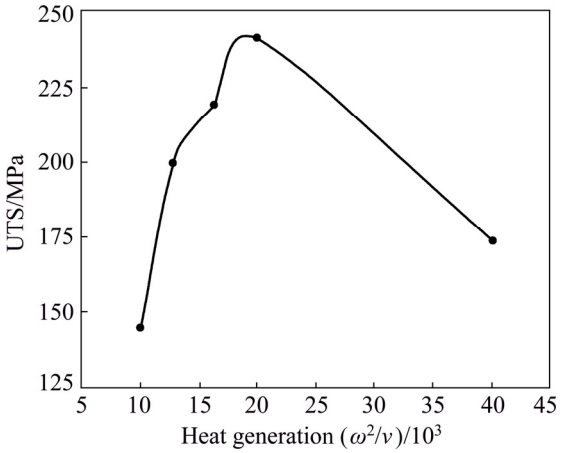

Fig. 14 Relationship between tensile strength and heat generation for FSWed specimens

BISADI et al [15] investigated the influence of heat generation on mechanical properties of FSWed commercially pure copper and Al5083 alloy joint. They reported that the UTS mostly decreased by the rising of the heat input generated by tool rotation. As mentioned above, the increase of the IMCs by elevating the welding temperature led to a reduction in the UTS. The formation of IMCs increases by increasing the ω^2/v value to about 20000 and decreases at high heat generations.

The elongation and UTS of the 1000-100p specimen were 1.67% and 143 MPa, respectively. The UTS of the 800-50p, 900-50p, and 1000-50p specimens increased by increasing the heat generation and reached 200, 219 and 239 MPa, respectively. The elongation of the 800-50p, 900-50p, and 1000-50p specimens increased to 2.61%, 3.95% and 5.09%, respectively. By further enhancement in the heat input of 1000-25p specimen, the elongation and UTS were decreased and reached 2.72% and 174 MPa, respectively. The low UTS for 1000-100 specimens is probably related to the high tool traverse speed. Therefore, the flow of material and the mixing of copper and aluminum did not occur appropriately.

The decelerated traverse speed for 800-50p specimen was compared to that of 1000-100p

specimen, resulting in a drastic increase in UTS value. ARGESI et al [36] reported that the increase in UTS is related to fine grains in the SZ, according to the Hall−Patch equation. However, the low rotation speed resulted in a non-appropriate distribution of the nano-sized SiC particles in the SZ and, consequently, brittle fracture in this region.

For the case of 900-50p and 1000-50p specimens, an increase in the rotation speed of the tool resulted in an increase in the UTS, so that for the 1000-50p sample, the UTS reached 92% strength of the base aluminum. As it is evident from Fig. 3, an appropriate mixing process and excellent material flow between copper and aluminum occurred. The 1000-50p specimen has the best tensile properties due to the small grains and appropriate distribution of nano-particles in the stir zone. An increase in the tool rotation speed resulted in an improvement in the distribution of the nano-particles and, consequently, led to the transmission failure of SZ to TMAZ. The formation of nano-composite in the SZ improved the stress transfer from the matrix to the reinforcement particles and increased the tensile strength. ABDOLAHZADEH et al [27] reported that in the FSW process, the TMAZ, experiences severe deformation, which results in TMAZ dislocations. In other words, the deformation causes further dislocations and results in crack nucleation. In the tensile experiment, the dislocations accumulated more quickly than the base metal, which results in nucleation of crack and failures of TMAZ [27,44].

For the 1000-25p specimen, the heat generation significantly increased and reduced the UTS compared to the 1000-50p specimen. Due to the extent of increase in heat generation, the tensile strength will be dependent on IMCs. The amount of IMCs is increased upon an increase in heat generation. LIU et al [45] reported that the formation of IMCs in the SZ reduces the FSWed joint's ductility, and this is basically due to the inherent nature of IMCs, which reduces the YS, UTS and elongation. On the other hand, exceeding the heat generation to high amount may decrease UTS via the creation of defects.

As it is obvious from the results, the 1000-50p specimen illustrated the best tensile properties due to its moderate heat generation, which resulted in the production of a lower amount of IMCs and excellent distribution of SiC nano-particles and their pinning effect on the grain boundaries, which led to the grain refining in the microstructure.

Figure 15 illustrates the SEM images of the fracture surfaces of 1000-100p, 900-50p, 1000-50p and 1000-50 FSWed specimens. Notably, no dimples were observed on the fracture surface of the 1000-100p specimen. This is due to the inadequate mixing of aluminum and copper. On the other hand, the incorporation of nano-particles was not appropriate due to high traverse speeds and,

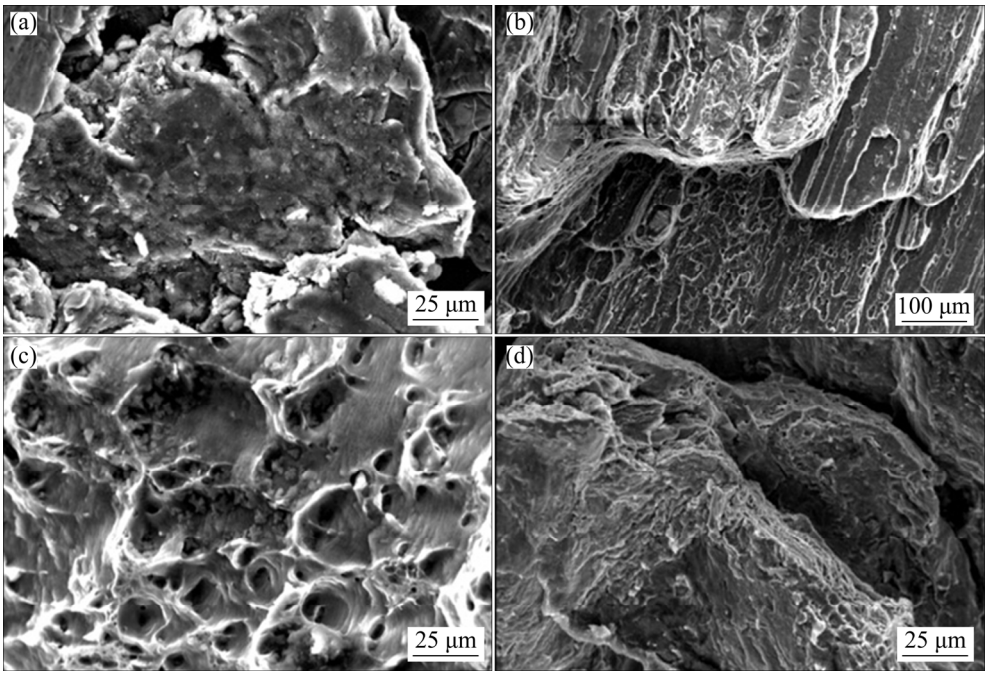

Fig. 15 SEM images of fracture surface of FSWed specimens: (a) 1000-100p; (b) 900-50p; (c) 1000-50p; (d) 1000-50

thus, the nano-particles are agglomerated. Therefore, the fracture mode of this sample was brittle. In the 1000-50p specimen, some dimples are present in the structure, which indicates the ductile fracture. A smooth surface with some small dimples is obvious on the fracture surface of 900-50p and 1000-50 specimens. Moreover, some cleavage planes with tearing edges could be observed on their fracture surface. Therefore, these two specimens tend to have a brittle mode fracture.

The XRD analysis for the fracture surface of the 1000-100p specimen is shown in Fig. 16, which indicates that the IMCs formed in these specimens. As it is evident, many intermetallic systems with varying hardness could be formed under different working conditions and temperatures between Al and Cu. Thus, in addition to the mentioned compounds, other intermetallic compounds may also be formed. However, the XRD and EDS analysis could only detect Al_4Cu_9 and Al_2Cu intermetallic compounds in the stir zone of the samples, as reported in Ref. [36]. Figure 16 also approves the existence of SiC nano-particles on the fracture surface of specimens. Because of the presence of nano-particles and the formation of IMCs in the joints, most failure modes were brittle.

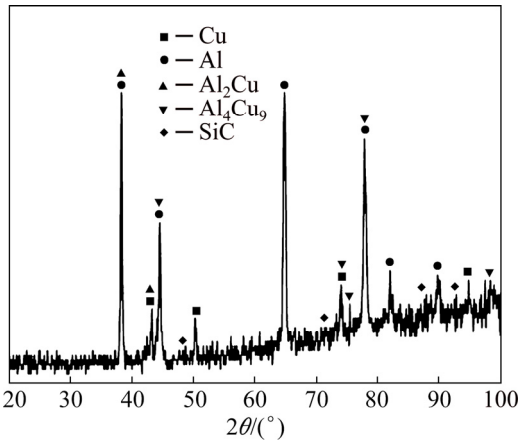

Fig. 16 XRD analysis of fracture surface of 1000-100p specimen

3.4.2 Microhardness

The microhardness profile of FSWed specimens that were carried out in the middle of their cross-section, is illustrated in Fig. 17. As it is clear, the base microhardness of pure copper plate and AA5754-H114 alloy are HV120 and HV62, respectively. The microhardness of the welded aluminum−copper joint with the addition of reinforcing SiC nano-particles is directly related to the grain size, density of dislocations, and the amount of reinforcing particles and IMCs.

It has been reported by LEE et al [41] that, according to the Hall−Petch equation, the microhardness increases by decreasing grain size, revealing that the dislocations created due to the differences between thermal expansion coefficients of aluminum, copper, and SiC nano-particles, led to increasing the microhardness. The addition of reinforcing SiC nano-particles increases the microhardness for two reasons, i.e., the hard nature of SiC nano-particles, and the pinning effect of the grain boundaries [22,30]. The high heat generation increases the formation of the IMCs, which increases the microhardness.

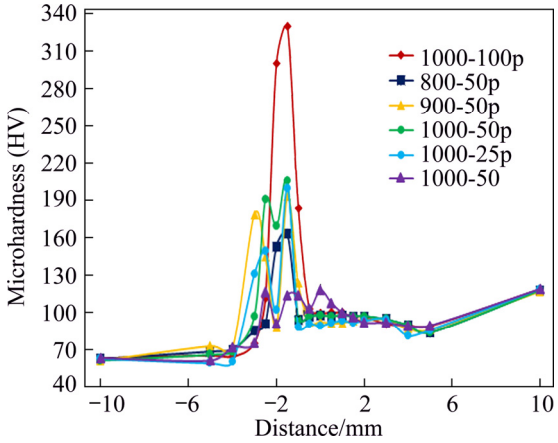

Fig. 17 Microhardness profile of FSWed specimens

Therefore, among the cases cited above, selecting the most significant and influential factor in microhardness is complicated. However, it should be noted that the presence of hard SiC nano-particles, could reduce the grain size in the SZ, and also, the formation of IMCs will result in increased microhardness. SUN and FUJII [30] reported that the increase in hardness of FSWed copper with the incorporation of SiC nano-particles is supposed to be contributed by decrease in the average grain size via the Zener pinning effect and the existence of the SiC nano-particles with a high hardness.

The maximum microhardness in 1000-100p specimen was HV320. Due to the role of SiC reinforcement nano-particles, the thermal mismatch between the Al matrix and SiC nano-particles led to high dislocation density. Also, SiC nano-particles have high hardness and resistance to plastic

deformation during indentation, which resulted in increased hardness [23]. Besides, as observed in Fig. 9(d), the SiC nano-particles are agglomerated in the SZ due to the high tool speed. These hard SiC nano-particles lead to increase in the microhardness.

On the other hand, this may also be related to the presence of IMCs. The existence of hard and brittle IMCs in the SZ resulted in more intense hardness peaks. According to the mentioned cases, it can be concluded that the synergic effect of SiC nano-particles and IMCs will result in an increase in the microhardness peak.

BAHRAMI et al [22] have reported that the highest hardness will result in high aggregation of nano-sized SiC particles. Thus, in the case of 800-50p, 900-50p and 1000-50p specimens, the distribution of SiC nano-particles improved by increasing the tool rotation speed, and consequently, the maximum microhardness is decreased. In the 1000-50 specimen without SiC nano-particles, the microhardness was much lower than the other specimens. Furthermore, reinforcing SiC nano-particles resulted in increased microhardness through the Hall−Petch equation and high hardness of SiC. Moreover, the formation of SiC-rich and SiC-free regions and the IMCs formation resulted in fluctuations of microhardness in the SZ. SUN and FUJII [30] also reported that the low hardness values achieved in some areas are related to the particles-free areas in the stir zone.

4 Conclusions

(1) An increase in heat generation resulted in an enhancement in the grain size and significantly promoted the number of IMCs. The formation of Al_4Cu_9 and Al_2Cu intermetallic compounds in the stir zone was established. The grain sizes of aluminum and copper in the SZ were also reduced from the 38.3 and 12.4 to 12.9 and 5.1 μm, in the presence of nano-sized SiC particles.

(2) The highest tensile strengths were obtained in joints prepared by 50 mm/min travel speed and 1000 r/min rotation speed, as it was 239 MPa (i.e., 92% of the strength of aluminum base). Addition of the reinforcing SiC nano-particles, increased the tensile strength from 169 to 239 MPa. The addition of the SiC nano-particles led to fine grains size in the SZ and increased both the pinning effects and the tensile strength.

(3) Microhardness of the friction stir welded copper−aluminum joints was directly related to the amount of reinforcing SiC nano-particles, intermetallic compounds, and grain size. The highest microhardness of SZ in the absence of SiC nano-particles was HV120, which significantly increased to HV320 in the presence of SiC nano-particles, for the 1000-100p specimen. The synergic effect of SiC nano-particles and IMCs resulted in an increase in the microhardness peak.

References

[1] TAN C, JIANG Z, LI L, CHEN Y, CHEN X. Microstructural evolution and mechanical properties of dissimilar Al−Cu joints produced by friction stir welding [J]. Materials & Design, 2013, 51: 466−473.

[2] AKINLABI E T, ANDREWS A, AKINLABI S A. Effects of processing parameters on corrosion properties of dissimilar friction stir welds of aluminium and copper [J]. Transactions of Nonferrous Metals Society of China, 2014, 24: 1323−1330.

[3] MUBIAYI M P, AKINLABI E T. Evolving properties of friction stir spot welds between AA1060 and commercially pure copper C11000 [J]. Transactions of Nonferrous Metals Society of China, 2016, 26: 1852−1862.

[4] MUTHU M F X, JAYABALAN V. Effect of pin profile and process parameters on microstructure and mechanical properties of friction stir welded Al−Cu joints [J]. Transactions of Nonferrous Metals Society of China, 2016, 26: 984−993.

[5] SAHU P K, PAL S, PAL S K, JAIN R. Influence of plate position, tool offset and tool rotational speed on mechanical properties and microstructures of dissimilar Al/Cu friction stir welding joints [J]. Journal of Materials Processing Technology, 2016, 235: 55−67.

[6] ZHANG Q Z, GONG W B, WEI L. Microstructure and mechanical properties of dissimilar Al−Cu joints by friction stir welding [J]. Transactions of Nonferrous Metals Society of China, 2015, 25: 1779−1786.

[7] LI X W, ZHANG D T, CHENG Q, ZHANG W. Microstructure and mechanical properties of dissimilar pure copper/1350 aluminum alloy butt joints by friction stir welding [J]. Transactions of Nonferrous Metals Society of China, 2012, 22: 1298−1306.

[8] MUTHU M F X, JAYABALAN V. Tool travel speed effects on the microstructure of friction stir welded aluminum–copper joints [J]. Journal of Materials Processing Technology, 2015, 217: 105−113.

[9] ABDOLLAH-ZADEH A, SAEID T, SAZGARI B. Microstructural and mechanical properties of friction stir welded aluminum/copper lap joints [J]. Journal of Alloys and Compounds, 2008, 460: 535−538.

[10] OUYANG J, YARRAPAREDDY E, KOVACEVIC R. Microstructural evolution in the friction stir welded 6061

aluminum alloy (T6-temper condition) to copper [J]. Journal of Materials Processing Technology, 2006, 172: 110−122.

[11] AL-JARRAH J A. Surface morphology and mechanical properties of aluminum−copper joints welded by friction stir welding [D]. Jordan: Al-Balqa Applied University, 2014.

[12] MISHRA R S, DE P S, KUMAR N. Friction stir welding and processing [J]. Switzerland: Springer International Publishing, 2014.

[13] PISHEVAR M, MOHANDESI J A, OMIDVAR H, SAFARKHANIAN M. Influences of friction stir welding parameters on microstructural and mechanical properties of AA5456 (AlMg5) at different lap joint thicknesses [J]. Journal of Materials Engineering and Performance, 2015, 24: 3835−3844.

[14] YU C, HUA D, LI J Z, ZHAO J W, FU M J, LI X H. Effect of welding heat input and post-welded heat treatment on hardness of stir zone for friction stir-welded 2024-T3 aluminum alloy [J]. Transactions of Nonferrous Metals Society of China, 2015, 25: 2524−2532.

[15] BISADI H, TAVAKOLI A, SANGSARAKI M T, SANGSARAKI K T. The influences of rotational and welding speeds on microstructures and mechanical properties of friction stir welded Al5083 and commercially pure copper sheets lap joints [J]. Materials & Design, 2013, 43: 80−88.

[16] HUANG Y, XIE Y, MENG X, LI J, ZHOU L. Joint formation mechanism of high depth-to-width ratio friction stir welding [J]. Journal of Materials Science & Technology, 2019, 35: 1261−1269.

[17] HUANG Y, XIE Y, MENG X, LV Z, CAO J. Numerical design of high depth-to-width ratio friction stir welding [J]. Journal of Materials Processing Technology, 2018, 252: 233−241.

[18] MEHTA K P, BADHEKA V J. A review on dissimilar friction stir welding of copper to aluminum: Process, properties, and variants [J]. Materials and Manufacturing Processes, 2016, 31: 233−254.

[19] BARMOUZ M, ASADI P, GIVI M B, TAHERISHARGH M. Investigation of mechanical properties of Cu/SiC composite fabricated by FSP: Effect of SiC particles' size and volume fraction [J]. Materials Science and Engineering A, 2011, 528: 1740−1749.

[20] BASSANI P, CAPELLO E, COLOBMO D, PREVITALI B, VEDANI M. Effect of process parameters on bead properties of A359/SiC MMCs welded by laser [J]. Composites: Part A Applied Science and Manufacturing, 2007, 38: 1089−1098.

[21] SHAMSIPUR A, KASHANI-BOZORG S F, ZAREI-HANAKI A. Production of in-situ hard Ti/TiN composite surface layers on CP−Ti using reactive friction stir processing under nitrogen environment [J]. Surface and Coating Technology, 2013, 218: 62−70.

[22] BAHRAMI M, DEHGHANI K, GIVI M K B. A novel approach to develop aluminum matrix nano-composite employing friction stir welding technique [J]. Materials & Design, 2014, 53: 217−225.

[23] BAHRAMI M, GIVI M K B, DEHGHANI K, PARVIN N. On the role of pin geometry in microstructure and mechanical properties of AA7075/SiC nano-composite fabricated by friction stir welding technique [J]. Materials & Design, 2014, 53: 519−527.

[24] BAHRAMI M, NIKOO M F, GIVI M K B. Microstructural and mechanical behaviors of nano-SiC-reinforced AA7075-O FSW joints prepared through two passes [J]. Materials Science and Engineering A, 2015, 626: 220−228.

[25] PANTELIS D, KARAKIZIS P, DANIOLOS N, CHARITIDIS C, KOUMOULOS E, DRAGATOGIANNIS D. Microstructural study and mechanical properties of dissimilar friction stir welded AA5083-H111 and AA6082-T6 reinforced with SiC nanoparticles [J]. Materials and Manufacturing Processes, 2016, 31: 264−274.

[26] KARTHIKEYAN P, MAHADEVAN K. Investigation on the effects of SiC particle addition in the weld zone during friction stir welding of Al 6351 alloy [J]. The International Journal of Advanced Manufacturing Technology, 2015, 80: 1919−1926.

[27] ABDOLLAHZADEH A, OMIDVAR H, SAFARKHANIAN M A, BAHRAMI M. Studying microstructure and mechanical properties of SiC-incorporated AZ31 joints fabricated through FSW: The effects of rotational and traveling speeds [J]. The International Journal of Advanced Manufacturing Technology, 2014, 75: 1189−1196.

[28] ABBASI M, ABDOLLAHZADEH A, OMIDVAR H, BAGHERI B, REZAEI M. Incorporation of SiC particles in FS welded zone of AZ31 Mg alloy to improve the mechanical properties and corrosion resistance [J]. International Journal of Materials Research, 2016, 107: 566−572.

[29] BODAGHI M, DEHGHANI K. Friction stir welding of AA5052: The effects of SiC nano-particles addition [J]. The International Journal of Advanced Manufacturing Technology, 2017, 88: 2651−2660.

[30] SUN Y, FUJII H. The effect of SiC particles on the microstructure and mechanical properties of friction stir welded pure copper joints [J]. Materials Science and Engineering A, 2011, 528: 5470−5475.

[31] KARAKIZIS P, PANTELIS D, FOURLARIS G, TSAKIRIDIS P. Effect of SiC and TiC nanoparticle reinforcement on the microstructure, microhardness, and tensile performance of AA6082-T6 friction stir welds [J]. The International Journal of Advanced Manufacturing Technology, 2018, 95: 3823−3837.

[32] FALLAHI A, SHOKUHFAR A, OSTOVARI MOGHADDAM A, ABDOLAHZADEH A. Analysis of SiC nano-powder effects on friction stir welding of dissimilar Al−Mg alloy to A316L stainless steel [J]. Journal of Manufacturing Processes, 2017, 30: 418−430.

[33] ABDOLLAHZADEH A, SHOKUHFAR A, CABRERA J M, ZHILYAEV A P, OMIDVAR H. In-situ nanocomposite in friction stir welding of 6061-T6 aluminum alloy to AZ31 magnesium alloy [J]. Journal of Materials Processing Technology, 2019, 263: 296−307.

[34] MORADI M, JAMSHIDI AVAL H, JAMAATI R. Effect of pre and post welding heat treatment in SiC-fortified dissimilar AA6061-AA2024 FSW butt joint [J]. Journal of Manufacturing Processes, 2017, 30: 97−105.

[35] GUAN M, WANG Y H, HUANG Y X, LIU X, MENG X C, XIE Y M, LI J C. Non-weld-thinning friction stir welding [J]. Materials Letters, 2019, 255: 126506.

[36] ARGESI F B, SHAMSIPUR A, MIRSALEHI S E. Dissimilar joining of pure copper to aluminum alloy via friction stir welding [J]. Acta Metallurgica Sinica (English Letters), 2018, 31: 1183−1196.
[37] DAS H, MONDAL M, HONG S T, CHUN D M, HAN H N. Joining and fabrication of metal matrix composites by friction stir welding/processing [J]. International Journal of Precision Engineering and Manufacturing — Green Technology, 2018, 5: 151−172.
[38] ABDOLLAHZADEH A, SHOKUHFAR A, CABRERA J M, ZHILYAEV A P, OMIDVAR H. The effect of changing chemical composition on dissimilar Mg/Al friction stir welded butt joints using zinc interlayer [J]. Journal of Manufacturing Processes, 2018, 34: 18−30.
[39] SAREMI M L, MIRSALEHI S E, SHAMSIPUR A. Investigation on metallurgical structure and mechanical properties of dissimilar Al 2024/Cu FSW T-joints [J]. Transactions of the Indian Institute of Metals, 2017, 70: 1869−1877.
[40] VERMA S, MISRA J. Study on temperature distribution during friction stir welding of 6082 aluminum alloy [J]. Materials Today: Proceedings, 2017, 4: 1350−1356.
[41] LEE W B, BANG K S, JUNG S B. Effects of intermetallic compound on the electrical and mechanical properties of friction welded Cu/Al bimetallic joints during annealing [J]. Journal of Alloys and Compounds, 2005, 390: 212−219.
[42] GALVAO I, OLIVERIA J, LOUREIRO A, RODRIGUES D. Formation and distribution of brittle structures in friction stir welding of aluminium and copper: Influence of process parameters [J]. Science and Technology of Welding and Joining, 2011, 16: 681−689.
[43] DIETER G E, BACON D. Mechanical metallurgy [M]. New York: McGraw-Hill, 1986.
[44] ABDOLLAHZADEH A, SHOKUHFAR A, OMIDVAR H, CABRERA J M, SOLONIN A, OSTOVARI A, ABBASI M. Structural evaluation and mechanical properties of AZ31/SiC nano-composite produced by friction stir welding process at various welding speeds [J]. Journal of Materials: Design and Applications, 2019, 233: 831−841.
[45] LIU H J, SHEN J J, ZHOU L, ZHAO Y Q, LIU C, KUANG L Y. Microstructural characterisation and mechanical properties of friction stir welded joints of aluminium alloy to copper [J]. Science and Technology of Welding and Joining, 2011, 16: 92−98.

异种搅拌摩擦焊制备铜铝合金双金属纳米复合材料

Farhad BAKHTIARI ARGESI, Ali SHAMSIPUR, Seyyed Ehsan MIRSALEHI

Department of Mining and Metallurgical Engineering, Amirkabir University of Technology, Tehran, Iran

摘　要：对纯铜与 AA5754 合金进行对接搅拌摩擦焊接。为了降低金属间化合物的有害影响，在搅拌摩擦焊(FSW)接头中添加纳米 SiC 强化颗粒。采用拉伸试验、显微硬度试验、扫描电镜和 X 射线衍射分析方法研究焊接接头的性能。结果显示，当焊接速度为 50 mm/min、转速为 1000 r/min 时接头的性能最好。纳米 SiC 颗粒的存在使搅拌区(SZ)铝和铜的晶粒尺寸分别从 38.3 和 12.4 μm 减小到 12.9 和 5.1 μm。含 SiC 纳米增强颗粒的接头其抗拉强度约为 240 MPa，是铝基体的~90%。且添加 SiC 纳米颗粒使接头焊缝区的最高显微硬度从 HV 160 显著增加到 HV 320。结果还表明，FSW 接头中生成热的升高使 Al_4Cu_9 和 Al_2Cu 金属间化合物的数量增加。

关键词：搅拌摩擦焊；异种 Al/Cu 接头；SiC 纳米颗粒；金属间化合物；显微组织特性；力学性能

(Edited by Xiang-qun LI)